

Learning Depth Vision-Based Personalized Robot Navigation From Dynamic Demonstrations in Virtual Reality

Jorge de Heuvel

Nathan Corral

Benedikt Kreis

Maren Bennewitz

Abstract—For the best human-robot interaction experience, the robot’s navigation policy should take into account personal preferences of the user. In this paper, we present a learning framework complemented by a perception pipeline to train a depth vision-based, personalized navigation controller from user demonstrations. Our refined virtual reality interface enables the demonstration of robot navigation trajectories under motion of the user for dynamic interaction scenarios. In a detailed analysis, we evaluate different configurations of the perception pipeline. As the experiments demonstrate, our new pipeline compresses the perceived depth images to a latent state representation and, thus, enables efficient reasoning about the robot’s dynamic environment to the learning. We discuss the robot’s navigation performance in various virtual scenes by enrolling a variational autoencoder in combination with a motion predictor and demonstrate the first personalized robot navigation controller that solely relies on depth images.

I. INTRODUCTION

The personalization of robots will be a key factor for comfortable and satisfying human-robot-interactions. As the integration of robots at home or at work will inevitably increase, the number one goal should be a naturally collaborative experience between users and the robot. However, users might have personal preferences about specific aspects of the robot’s behavior that define the personal golden standard of interaction. Falling short of user’s preferences could lead to negative interaction experiences and consequently frustration [1].

Where humans share the same environment with a mobile robot, the robot’s navigation behavior significantly influences the comfort of interaction [2]. Consequently, basic obstacle avoidance approaches are insufficient to address individual preferences such as proxemics, trajectory shape, or area of navigation in a given environment, while being a key component to a successful navigation without question. Instead, a robot’s navigation policy should be aware of the human [3] and reflect the human’s personal preferences.

Recent advances in user-focused robot navigation have paved the way to personalized navigation controllers [2]. More specifically, a virtual reality interface paired with a reinforcement learning framework enables the demonstration and training of highly customizable navigation behaviors. Even at the cost of slightly longer robot trajectories, the resulting navigation controller outperformed non-personalized controllers in terms of perceived comfort and interaction experience. However, a key assumption in the previous work

All authors are with the Humanoid Robots Lab, University of Bonn, Germany. This work has partially been funded by the Deutsche Forschungsgemeinschaft (DFG, German Research Foundation) under the grant number BE 4420/2-2 (FOR 2535 Anticipating Human Behavior).

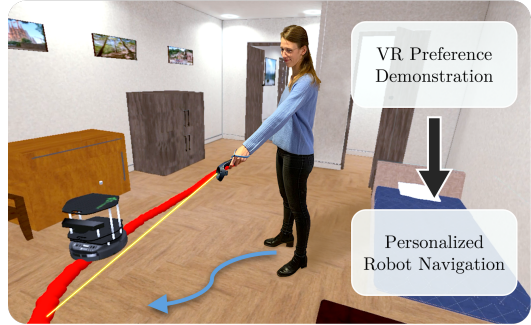


Fig. 1. Our virtual reality interface allows the demonstration of robot navigation preferences by drawing trajectories intuitively onto the floor. Using a learning-based framework, we achieve personalized navigation using a depth vision perception pipeline.

is an always-present, static human of known pose in a pre-defined environment with pose-encoded obstacles. This benefits the learning process with a low-dimensional and straightforward state space. To overcome the given assumptions, enrolling a depth vision sensor to sense both human and obstacles is a possible solution [4]. However, depth vision cameras come at the cost of high-dimensional, complex and redundant output. Learning from such high-dimensional output on dynamic scenes is indeed a challenging task [5]. The question crystallizes, how do we teach preferences of moving users in realistic environments, while relying on state-of-the art sensor-modalities?

To solve the challenges above, we introduce a depth vision-based perception pipeline that is both lightweight, human-aware and, most importantly, provides the robot with a low-dimensional representation of the dynamic scene. This pipeline i) detects the human and obstacles, ii) compresses the perceived depth information, and iii) enables efficient reasoning about the robot’s dynamic environment to the learning framework. To teach navigation preferences for scenarios in which not only the robot but also the human is moving, we advance our virtual reality interface and learning framework for dynamic navigation scenarios. Subsequently, we successfully train a navigation controller that closely reflects the demonstrated behavior, even for dynamic scenarios.

In summary, the **main contributions** of our study are:

- Learning a preference-reflecting navigation controller that relies solely on depth vision.
- A VR demonstration framework to record navigation preferences under dynamic human motion.
- An in-depth analysis of different perception configura-

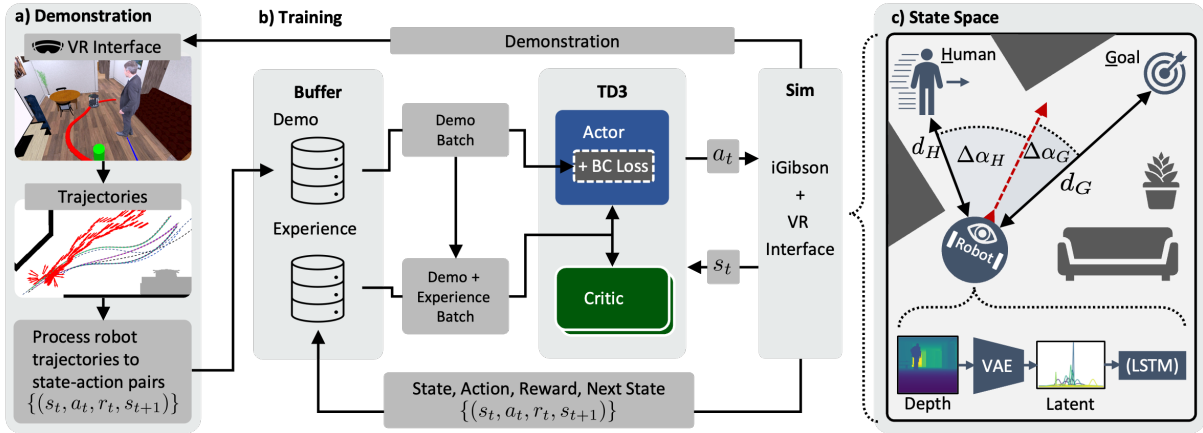


Fig. 2. Schematic representation of our architecture. **a)** Demonstration trajectories are drawn by the user in virtual reality onto the floor using the handheld controller. Subsequently, the trajectories are fed into the demonstration buffer. **b)** Our TD3 reinforcement learning architecture with an additional behavioral cloning (BC) loss on the actor trains a personalized navigation policy that outputs linear and angular velocities. The learned policy is transferred to a real robot. **c)** The robot-centric state space relies on a depth vision perception pipeline, capturing the vicinity of the human and obstacles in the environment, as well as the relative goal position. A variational autoencoder (VAE) compresses the raw images to a latent state representation, while a predictor (LSTM) provides subsequent state predictions as an option.

tions for personalized navigation.

II. RELATED WORK

Adjusting or learning the navigation behavior of a robot based on feedback or demonstration has been the focus of various studies [6], [7]. Especially, deep learning-based approaches shine by their ability to learn from subtle and implicit features in their environment [8], [9], [10]. This is a perfect prerequisite to use a deep reinforcement learning architecture for our personalized navigation controller.

Fusing the potential of user demonstrations with a learning architecture lead to promising results in the field of robotic manipulation tasks [11]. Therefore, this is a key concept for our learning architecture and has proven success in the field of robot navigation [2].

Vision-based sensor modalities for navigation appeal due to their cost-efficiency. For human-aware navigation, the detection and explicit localization of pedestrians has lead to socially-conform navigation controllers [4], [12].

Recent advances in the field of depth vision-based navigation in combination with reinforcement learning have been made by Hoeller *et al.* [13], who study a state representation of depth-images to efficiently learn navigation in dynamic environments. Our proposed perception pipeline is built upon their successful architecture.

Furthermore, a navigating agent benefits from dynamic scene understanding. Predicting the movement of surrounding pedestrians and obstacles with Long Short-Term Memory (LSTM) models has lead to promising results [14], [15], [13]. Therefore, we will adapt an LSTM architecture for our perception pipeline.

While in our previous work [2], we presented one of the first approaches at the intersection of both navigation and robot personalization, we now enhance the system by allowing to demonstrate navigation trajectories under dynamic motions and using only depth vision as input.

III. PROBLEM DEFINITION AND ASSUMPTIONS

In this work, we consider a robot navigating in the same room as a single, human user. The user has personal preferences about the way the robot circumnavigates him/her while pursuing a local goal in the same room. Such preferences could lie in the approaching behavior or the robot's trajectory shape. We explicitly do not consider multi-room navigation but assume that a local goal is provided from a global planner. The local goal could be a door on the opposite side of the current room to be traversed, or a location of interest in the same room. Using such sparse local goals several meters apart, we provide the controller with the spatial and temporal freedom to navigate towards the goal in a user-preferred personalized manner. A single human shares the navigation space with the robot, whether being dynamic by walking through the room, or resting static. To achieve user-preferred and collision-free navigation behavior, the robot relies only on an depth vision camera to sense the distance to the human as well as obstacles. We formulate personalized navigation as a learning task, where the robot learns a personalized controller outputting linear and angular velocity from virtual reality demonstrations of the user.

A. Learning Architecture

The learning approach presented in this section is a hybrid of reinforcement learning (RL) and behavior cloning (BC).

Reinforcement learning refers to the optimization of environment interactions, leading from state $s_t \rightarrow s_{t+1}$ that obey a Markov Decision Process. The interacting agent receives a reward $r_t = r(s_t, a_t)$ for taking an action $a_t = \pi_\phi(s_t)$ at time step t with respect to a policy π_ϕ . The tuples (s_t, a_t, r_t, s_{t+1}) are referred to as state-action pairs. The optimization goal is to maximize the overall return $R = \sum_{i=t}^T \gamma^{(i-t)} r_t$ of the γ -discounted rewards, onward from time step t .

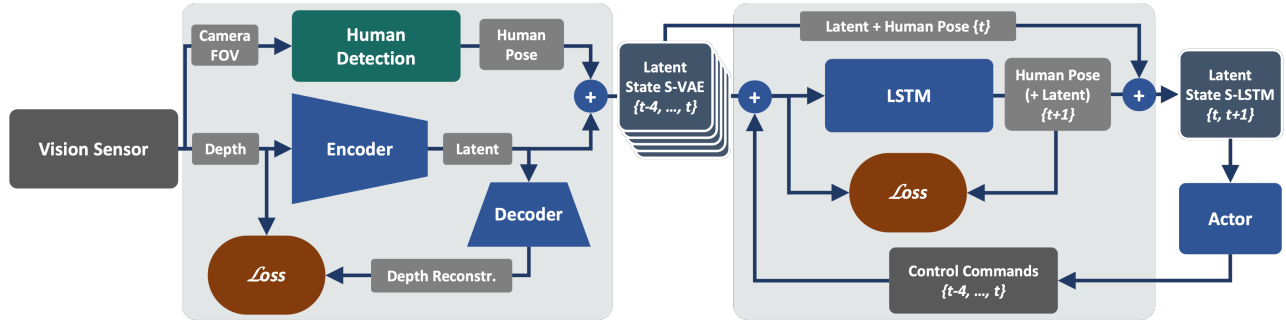


Fig. 3. Schematic representation of the perception pipeline. **Left:** The vision sensor’s depth frames are compressed with a VAE. In parallel, we check for human presence in the sensor’s field of view (FOV), in which case we provide the human position relative to the robot. The merged latent state S-VAE provides our first state representation for learning. **Right:** After the last five states $l_{S\text{-VAE}}\{t-4, \dots, t\}$ are merged with the robot control commands, the LSTM predicts both the next latent as well as the next human pose. Only the human pose prediction $(d_H^{t+1}, \Delta\alpha_H^{t+1})$ is merged with the previous latent l_t and human pose $(d_H^t, \Delta\alpha_H^t)$ to the state S-LSTM. Both state versions S-VAE and S-LSTM are used separately for training.

Building upon our previous work [2], we enroll an off-policy twin-delayed deep deterministic policy gradient (TD3) reinforcement learning architecture [16]. In short, two critics networks learn to estimate the value of the state distribution, the actor networks learn a policy $\pi(s_t) = a_t$ ideally leading to the highest expected return R . All three networks are multi-layer perceptrons (MLP) and share the same architecture. TD3’s continuous action space ensures smooth robot control, where the actor network outputs linear and angular velocities as control commands.

An additional modification to the standard TD3 is a behavioral cloning loss \mathcal{L}_{BC} on the actor network [11], besides the standard policy gradient loss $\nabla_\phi J$. The overall loss on the actor is $\nabla_\phi J_{\text{total}} = \lambda_{\text{RL}} \nabla_\phi J - \lambda_{\text{BC}} \nabla_\phi \mathcal{L}_{\text{BC}}$, where both parts can be balanced by controlling $\lambda_{\text{BC/RL}}$.

Furthermore, a separate buffer is introduced to provide demonstration data. The demonstration buffer is static and holds the state-action pairs of navigation preference demonstrations collected in virtual reality. Only those demonstrations are fed into the behavioral cloning loss.

Both the behavioral cloning loss and providing demonstration data throughout the training process ensure a learned navigation policy that exhibits demonstration like behavior whenever the navigation scenario allows. At the same time, the policy learns to deal with unknown states not covered by the demonstration data. During training, RL and BC complement each other. Fig. 2 depicts a schematic overview of our approach. For further details on the learning algorithm, please refer to [2].

B. Representation Learning

1) *Variational Autoencoder:* Reinforcement learning on raw high-dimensional vision data is unfeasible. Ideally, a dimensionality-reduced state representation is used [13]. Thus, we compress the depth data to a latent representation using a variational autoencoder (VAE). More precisely, we utilize a β -VAE with six relu-activated convolutional layers. The dimensionality reduction is factor 320 from a 128×80 pixel depth image to a latent space of dimensionality 32. To make the model robust against sensor noise that a

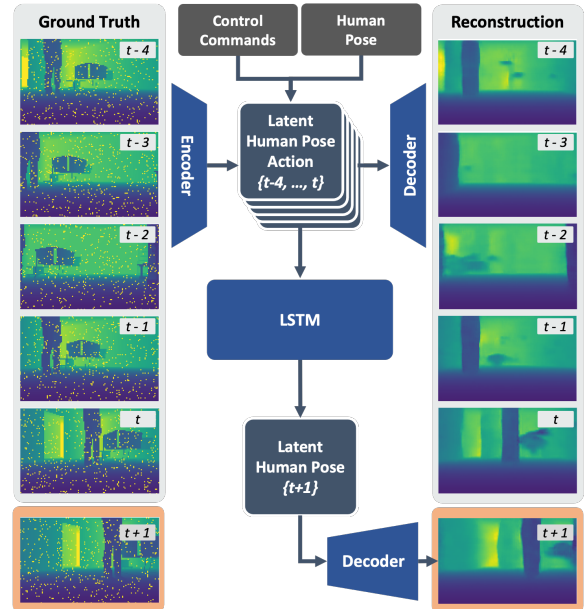


Fig. 4. Visualization of the trained VAE and LSTM model. **Left:** The ground truth depth frames of subsequent time steps are encoded using the VAE to a latent space of dimensionality 32. **Right:** The reconstruction using the decoder of the latent showcases the learned features and the VAE’s denoising performance. **Bottom:** The LSTM predicts the next latent and human pose, where the latent reconstruction is shown.

depth camera would exhibit, we apply a 5 % dropout noise to the depth frames during VAE training. The VAE learns to level out the noise, as the VAE’s reconstruction loss is computed between the decoded and the noise-free depth-frame. A visualization of the VAE’s performance is depicted in Fig. 3.

2) *Predictor:* Originating from single depth frames, the latent space alone fails to capture dynamic scene information such as motion or human movement. To leverage dynamic scene information such as the human motion for the navigation controller, a predictor is introduced. The predictor receives the last five human poses, control commands and latent frames $(d_H^i, \Delta\alpha_H^i, a_i, l_i)_{i \in \{t-4, \dots, t\}}$ as input. We predict the next human pose $(d_H^{t+1}, \Delta\alpha_H^{t+1})$ and the latent of the next

time-step l_{t+1} . The model consists of two LSTM layers with 64 units each, followed two linearly activated MLPs which output both mean μ_{t+1} and variance σ_{t+1} as in the VAE. Subsequently, the latent prediction l_{t+1} is sampled from μ_{t+1} and σ_{t+1} . The human pose prediction is performed by a two-layer MLP, taking the LSTM-layer's output as input. A visualization of the predictor's performance is depicted in Fig. 3 at the bottom.

C. Training Data

To train the autoencoder and predictor, we generate an extensive dataset of depth-frames in the iGibson simulator. Here, we use the scene setup described in IV-C with a static or dynamic human. The robot's navigation policy for the dataset generation is a simple obstacle avoidance controller trained with reinforcement learning. Furthermore, the dataset contains ground-truth data about the human pose and the human's presence in the sensor's field of view.

D. State and Action Space

Our robot-centric state space consists of three main parts, compare Fig. 2c: 1) The relative goal position, 2) the (predicted) human position and presence in the robot's field of view and 3) the latent representation of the depth data. Thus, the human is both implicitly encoded as an obstacle in the latent-encoded depth image, but also explicitly. All positions are given in polar coordinates relative to the robot's pose. The human presence in the camera's field of view is one-hot encoded with $k_H \in \{0, 1\}$, where the fallback values for the human position in the case of absence are ($d_H^* = -1$ m, $\Delta\alpha_H^* = 0$ rad). Given the state space as input, the trained controller will output forward and angular velocity (v, ω) as control commands. Hence, our action space is two-dimensional.

E. Reward

As introduced in our previous work [2], we aim to teach user-specific navigation preferences not by complex reward shaping, but only via demonstration data. Consequently, we keep the reward as sparse as possible besides basic collision penalties and goal rewards

$$r = r_{\text{collision}} + r_{\text{goal}} + r_{\text{timeout}}. \quad (1)$$

The scaling factor $c_{\text{rew}} = 10$ is used throughout the reward definition below. Upon collision with either an obstacle or the human, we penalize with

$$r_{\text{collision}} = \begin{cases} -\frac{1}{2}c_{\text{rew}} & \text{if collision} \\ 0 & \text{else.} \end{cases} \quad (2)$$

When the robot reaches the goal location, a positive reward is provided:

$$r_{\text{goal}} = \begin{cases} +c_{\text{rew}} & \text{if goal reached in demonstration data} \\ +\frac{c_{\text{rew}}}{2} & \text{if goal reached during training} \\ 0 & \text{else} \end{cases} \quad (3)$$

Note the explicitly higher reward of the demonstration data to boost the value of demonstration-like behavior for the critics during learning. This is complemented further by an additional $+\frac{c_{\text{rew}}}{100}$ on each demonstration state. In short, a higher value of demonstration-like behavior encourages user-preference-like navigation whenever possible, while preventing the agent from taking more efficient, shorter trajectories to achieve the faster and higher return R . For more details, please refer to [2].

Upon timeout where the goal is not reached by the agent after a certain number of steps N_{ep} , we penalize with

$$r_{\text{timeout}} = \begin{cases} -\frac{c_{\text{rew}}}{4} & \text{if episode timeout } (n > N_{\text{ep}}) \\ 0 & \text{else.} \end{cases} \quad (4)$$

It helps the agent to overcome navigation behavior that does not lead to the goal on the long run. An episode denotes the trajectory roll-out from initial robot placement until one of the termination criteria is satisfied. All three reward criteria are also termination criteria for an episode.

IV. DEMONSTRATION AND TRAINING ENVIRONMENT

We first introduce the advances on the virtual reality interface, in which a human user teaches personal navigation preferences to a robot - now under dynamic motion. Subsequently, the learning environment and navigation task are presented.

A. Simulator and Robot

To teach and train our navigation controller in a realistic environment, we use the iGibson simulator [17] that provides randomizable, interactive scenes of homes. iGibson renders the robot's vision sensors, which serve as input to our perception pipeline during training. Its underlying physics engine is Pybullet [18]. Furthermore, iGibson provides a VR interface that we used for immersive demonstration. We focus on a differential-wheeled robot and the robotic platform used both in simulation and real-world experiments is the Kobuki Turtlebot 2. Generally, our approach is applicable to other robots with similar control modalities. The Turtlebot's control limits lie at $v \in [0, 0.5]$ m s⁻¹ forward and $\omega \in [-\pi, +\pi]$ rad s⁻¹ angular. Inspired by the Intel Realsense D455 depth camera, the robot features a forward facing depth-camera with a 89° horizontal field of view. The depth-sensing range is limited to 6 m, which is equivalent to a temporal foresight of 12 s at the Turtlebot's maximum forward velocity. As there is no sensor facing backward to sense rear obstacles, the Turtlebot is not allowed to drive backward.

B. Collecting and Processing Demonstration Trajectories

The demonstration collection procedure is based on our previous work [2], with two major novelties: Whereas the human was previously static during demonstration, the demonstrating user can now move and teach dynamic situations. Additionally, we use the more realistic iGibson simulator with rich scenes. To demonstrate, the user firstly familiarizes him/herself with the environment in VR. Subsequently,

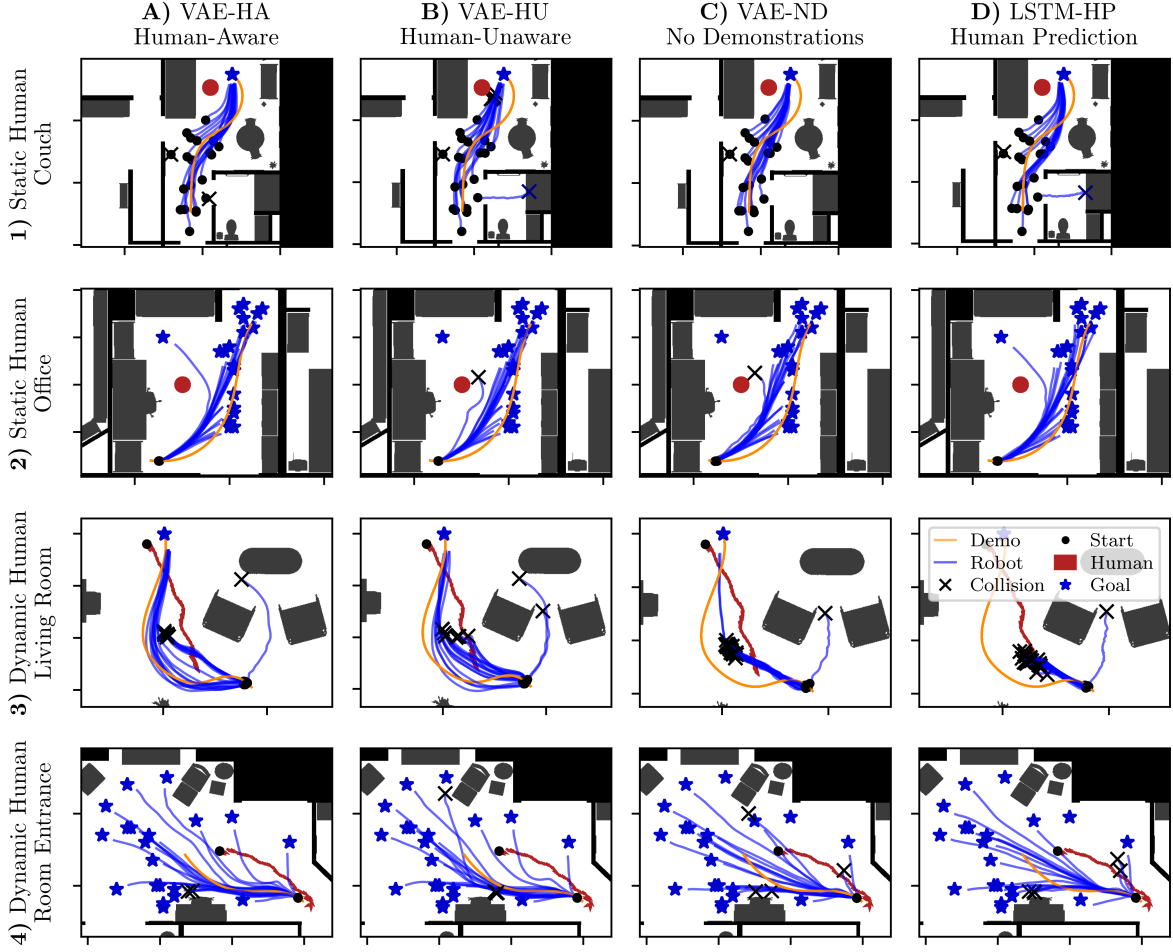


Fig. 5. The robot's learned navigation behavior for scenes, where preferences were demonstrated (**rows 1-4**) and perception as well as learning configurations (**columns A-D**) are depicted. For all scenes, the navigation preference as drawn demonstration trajectories are shown (orange). The human (red) is either static (red circle) or moving through the scene (red arrow). The robot's learned navigation paths are marked in blue. Goal (blue star) and start location (black dot) are either taken from the demonstration trajectory or sampled equivalently in the room across all configurations (columns). Collision locations are also indicated (black cross). In short, the VAE-HA approach (A) exhibits navigation behavior which is the closest to the demonstrated preferences. As the human-detection is turned off on the VAE-HU (B) and no human pose is provided to the controller, the robot performs less pronounced avoidance (B1 vs. A1). In contrast, the VAE-ND controller trained without any demonstration data (C) rather reflects a shortest path driving behavior.

he/she demonstrates a trajectory for the robot using the hand-held controller. There is no preset goal in the demonstration scene, but the goal location will automatically be set to the end of the demonstration trajectory. Now, as the robot executes the trajectory, the human position and orientation is recorded from the head-mounted display's location. So to complement the demonstration with his/her movement, the user can walk freely in the scene while the robot navigates. A wireless head-mounted display is clearly beneficial here. Just like the robot's trajectory, also the human trajectory is converted into a spline representation to be replayed during training and when the state-action for the demonstration buffer pairs are subsequently recorded. In a last step, the user can step aside and observe the moving robot together with a moving human 3D mesh from a third-person perspective. Based on the users evaluation, the demonstration is either kept or can be re-recorded.

The user study in our previous work has already shown great acceptance of our interface and perceived navigation comfort of the learned controller. Therefore, we focus on the refinement of the interface and development of a novel perception pipeline. So for this study, we record dynamic and static navigation scenarios by ourselves to develop and evaluate the new depth vision-based perception pipeline. The dataset contains 9 scene configurations, with around three demonstration trajectories each.

C. Navigation Task & Training

We train one single navigation controller on all scenes and demonstration scenarios. Start and goal location of the robot are randomly sampled in the same room, while ensuring a goal distance d_g between $1.5 \text{ m} < d < 6 \text{ m}$, equivalent to the depth sensing range. We can also setup the scene to replay the demonstration scenarios during training.

To simulate the human in the scene, four different behaviors are sampled: 1) Human walks in the opposite direction from the robot's goal to its start, thus encountering the robot. 2) Random human start and goal location in the same room. 3) Human moves according to recorded demonstrations. 4) Human is static. For modes 1+2, the human speed is sampled from a standard distribution $\mathcal{N}(\mu = 0.5 \text{ m s}^{-1}, \sigma = 0.3 \text{ m s}^{-1})$.

Lastly, we randomize over a set of iGibson scenes during training and change scenes every 50 episodes.

Before training begins, the replay buffer is initialized with 5×10^3 samples by executing randomly sampled actions. An overview on all relevant and experimentally obtained training parameters can be found in Tab. I.

V. EXPERIMENTAL EVALUATION

This section highlights the performance of our learned personalized navigation controller in a qualitative analysis.

A. Perception Pipeline Configurations

We evaluate different perception pipeline configurations against each other, compare Fig. 3. Their key differences lie in the state space as input to the RL policy.

The standard **human-aware** VAE-HA (Fig. 5A) state space configuration S-VAE contains the current latent depth encoding, goal position, the human presence binary and human position: $s_t^{\text{VAE-HA}} = (l_t, d_G, \Delta\alpha_G, k_H^t, d_H^t, \Delta\alpha_H^t)$.

The **human-unaware** VAE-HU (Fig. 5B) is the same controller as the VAE-HA in Fig. 5A, but the human presence in the robot's field of view is disabled in the state space and $k_H^t = 0, d_H^t = d_H^*, \Delta\alpha_H^t = \Delta\alpha_H^*$ during evaluation.

The **no-demonstration** VAE-ND controller does not rely on the learning architecture as shown in Fig. 2. It has neither a demonstration buffer, nor a behavioral cloning loss, making it a plain TD3 architecture. Therefore, it has learned its navigation behavior without user demonstrations.

The **human-prediction** LSTM-HP (Fig. 5D) state space configuration S-LSTM is similar to S-VAE, except the additional prediction of the next human position: $s_t^{\text{LSTM-HP}} = (s_t^{\text{VAE-HA}}, d_H^{t+1}, \Delta\alpha_H^{t+1})$. Therefore, S-LSTM provides a dynamic scene information by prediction the human movement.

TABLE I
NOTATIONS AND TRAINING SETTINGS.

Notation	Value	Description
β	3	Weighting factor of the VAE's KL-divergence
n_{ep}	150	Maximum number of steps per episode
B_E	2×10^5	Experience replay buffer size
$b_{E/D}$	64	Batch size of experience/demo data
l_a	1×10^{-4}	Learning rate of actor
l_c	8×10^{-4}	Learning rate of critic
γ	0.99	Discount factor
σ_{ϵ_π}	0.2	Std. deviation of exploration noise ϵ_π
σ_{ϵ_θ}	0.05	Std. deviation of target policy noise ϵ_θ
λ_{RL}	30/4	Weighting factor of RL gradient on actor
λ_{BC}	10/4	Weighting factor of BC loss gradient on actor

B. Qualitative Navigation Analysis

Fig. 5 shows the learned navigation behavior of our controller and highlights resulting differences between the perception pipeline configurations introduced above.

In Fig. 5.1, the human is static located at the couch. For the evaluation, the robot's start location is randomized, while keeping the goal at the end of the demonstration trajectory. As the robot traverses the living room, it shall navigate on the opposite side of the room close to the dining table and along the cupboard. With VAE-HA, the robot learned to navigate closely to the demonstrated preference. It exhibits a similar, smooth, S-shaped curve while passing by the couch. Interestingly, a pronounced difference in the robot's trajectory shape can be observed between VAE-HA and VAE-HU (Fig. 5.A1+B1). As the human is not explicitly observed in the state space, VAE-HU's approaching behavior to the human rather resembles shortest-path trajectories, while cutting short on the demonstrated S-shaped curve.

Located at the desk in Fig. 5.2., the static human prefers the robot to take a wide turn as it leaves the corner next to the desk. In this scenario, the navigation behavior among all configurations is similar. Also, no big difference between VAE-HA and VAE-HU can be observed. A possible explanation is the orientation of the robot to the human regarding the field of view (FOV). During most of the trajectory, the human will not be visible in the robot's FOV, resulting in little difference in the perception between VAE-HA and VAE-HU. Interestingly, controller VAE-ND learned to take a shortcut between the human and desk - a behavior that the demonstration-aware controllers avoid.

In Fig. 5.3, the moving human encounters the robot with an opposite direction of travel at the living room's suite. As a preference, the robot should take a wide turn of avoidance around the armchair to make space for the approaching human. Among all controllers, the navigation of the situation is challenging, leading to collisions around the armchair's corner. While the LSTM-HP fails to exhibit the demonstrated behavior in this scenario, VAE-HA and VAE-HU display successful preference-like avoidance behavior in some cases.

As the human walks out of the room in Fig. 5.4, the robot enters. When the robot detects the approaching human, it shall take a left turn and make room for the human to pass. When the human is out of its field of view, the robot can continue traversing the living room to its goal. In this scenario the effect of demonstration trajectories strikes: The VAE-ND controller without access to demonstrations mostly exhibits direct goal-oriented, straight-path navigation. Interestingly, the same applies for the LSTM-HP controller. The human collision avoidance behavior of VAE-HU suggests one interesting conclusion: Because of the human-unawareness, the characteristic S-shaped human-avoidance behavior when pursuing the goal across the human's path has to solely originate from the encoded depth information.

To conclude, the VAE-HA configuration leads to the best-performing personalized robot navigation controller. Interestingly, the LSTM-HP configuration does not seem to provide

a significant improvement compared to VAE-HA.

As demonstrated with our results, we successfully learn a personalized navigation controller that in most cases successfully navigates the environment, while reflecting demonstrated preferences in the trajectory shape. Our results let us draw the conclusion that personalized robot navigation based on depth vision sensors is possible.

VI. CONCLUSION

To summarize, we presented a learning approach to personalized navigation based on depth vision. We built upon the positive response to personalized navigation and to our virtual reality interface in our previously conducted user study [2]. This work enhanced the interface by allowing the user to intuitively demonstrate robot navigation preferences in dynamic human-robot navigation scenarios. With this work, we pave the path to personalized robot navigation based on a depth vision sensor architecture, hence overcoming key limitations of our previous work. As a next logical step, we will roll out our vision-based architecture to a real robot.

ACKNOWLEDGMENTS

We gratefully thank Marlene Wessels and Camilla Maslatón for their contribution on the motivational figure.

REFERENCES

- [1] T. Kruse, A. K. Pandey, R. Alami, and A. Kirsch, “Human-aware robot navigation: A survey,” vol. 61, no. 12, pp. 1726–1743. [Online]. Available: <https://www.sciencedirect.com/science/article/pii/S0921889013001048>
- [2] J. de Heuvel, N. Corral, L. Bruckschen, and M. Bennewitz, “Learning Personalized Human-Aware Robot Navigation Using Virtual Reality Demonstrations from a User Study,” in *2022 31th IEEE International Conference on Robot Human Interactive Communication (RO-MAN)*, pp. 898–905.
- [3] R. Möller, A. Furnari, S. Battiato, A. Härmä, and G. M. Farinella, “A survey on human-aware robot navigation,” vol. 145, p. 103837. [Online]. Available: <https://www.sciencedirect.com/science/article/pii/S0921889021001226>
- [4] C. Theodoridou, D. Antonopoulos, A. Kargakos, I. Kostavelis, D. Giakoumis, and D. Tzovaras, “Robot Navigation in Human Populated Unknown Environments based on Visual-Laser Sensor Fusion,” in *The15th International Conference on PErvasive Technologies Related to Assistive Environments*. ACM, pp. 336–342. [Online]. Available: <https://dl.acm.org/doi/10.1145/3529190.3534740>
- [5] M. Laskin, A. Srinivas, and P. Abbeel, “CURL: Contrastive Unsupervised Representations for Reinforcement Learning,” in *Proceedings of the 37th International Conference on Machine Learning*. PMLR, pp. 5639–5650. [Online]. Available: <https://proceedings.mlr.press/v119/laskin20a.html>
- [6] M. Kollmitz, T. Koller, J. Boedecker, and W. Burgard, “Learning Human-Aware Robot Navigation from Physical Interaction via Inverse Reinforcement Learning,” in *2020 IEEE/RSJ International Conference on Intelligent Robots and Systems (IROS)*. IEEE, pp. 11 025–11 031. [Online]. Available: <https://ieeexplore.ieee.org/document/9340865/>
- [7] X. Gao, X. Zhao, and M. Tan, “Modeling Socially Normative Navigation Behaviors from Demonstrations with Inverse Reinforcement Learning,” in *2019 IEEE 15th International Conference on Automation Science and Engineering (CASE)*. IEEE, pp. 1333–1340. [Online]. Available: <https://ieeexplore.ieee.org/document/8843123/>
- [8] M. Pfeiffer, S. Shukla, M. Turchetta, C. Cadena, A. Krause, R. Siegwart, and J. Nieto, “Reinforced Imitation: Sample Efficient Deep Reinforcement Learning for Mapless Navigation by Leveraging Prior Demonstrations,” vol. 3, no. 4, pp. 4423–4430. [Online]. Available: <https://ieeexplore.ieee.org/document/8458422/>
- [9] H. Karnan, A. Nair, X. Xiao, G. Warnell, S. Pirk, A. Toshev, J. Hart, J. Biswas, and P. Stone, “Socially Compliant Navigation Dataset (SCAND): A Large-Scale Dataset of Demonstrations for Social Navigation.” [Online]. Available: <http://arxiv.org/abs/2203.15041>
- [10] C. Chen, Y. Liu, S. Kreiss, and A. Alahi, “Crowd-Robot Interaction: Crowd-Aware Robot Navigation With Attention-Based Deep Reinforcement Learning,” in *2019 International Conference on Robotics and Automation (ICRA)*, pp. 6015–6022.
- [11] A. Nair, B. McGrew, M. Andrychowicz, W. Zaremba, and P. Abbeel, “Overcoming Exploration in Reinforcement Learning with Demonstrations,” in *2018 IEEE International Conference on Robotics and Automation (ICRA)*. IEEE, pp. 6292–6299. [Online]. Available: <https://ieeexplore.ieee.org/document/8463162/>
- [12] L. Tai, J. Zhang, M. Liu, and W. Burgard, “Socially Compliant Navigation Through Raw Depth Inputs with Generative Adversarial Imitation Learning,” in *2018 IEEE International Conference on Robotics and Automation (ICRA)*. IEEE, pp. 1111–1117. [Online]. Available: <https://ieeexplore.ieee.org/document/8460968/>
- [13] D. Hoeller, L. Wellhausen, F. Farshidian, and M. Hutter, “Learning a State Representation and Navigation in Cluttered and Dynamic Environments,” vol. 6, no. 3, pp. 5081–5088.
- [14] A. Alahi, K. Goel, V. Ramanathan, A. Robicquet, L. Fei-Fei, and S. Savarese, “Social LSTM: Human Trajectory Prediction in Crowded Spaces,” in *2016 IEEE Conference on Computer Vision and Pattern Recognition (CVPR)*. IEEE, pp. 961–971. [Online]. Available: <http://ieeexplore.ieee.org/document/7780479/>
- [15] T. Fernando, S. Denman, S. Sridharan, and C. Fookes, “Soft + Hardwired attention: An LSTM framework for human trajectory prediction and abnormal event detection,” vol. 108, pp. 466–478. [Online]. Available: <https://www.sciencedirect.com/science/article/pii/S0893608018302648>
- [16] S. Fujimoto, H. Hoof, and D. Meger, “Addressing Function Approximation Error in Actor-Critic Methods,” in *Proceedings of the 35th International Conference on Machine Learning*. PMLR, pp. 1587–1596. [Online]. Available: <https://proceedings.mlr.press/v80/fujimoto18a.html>
- [17] B. Shen, F. Xia, C. Li, R. Martín-Martín, L. Fan, G. Wang, C. Pérez-D'Arpino, S. Buch, S. Srivastava, L. Tchapmi, M. Tchapmi, K. Vainio, J. Wong, L. Fei-Fei, and S. Savarese, “iGibson 1.0: A Simulation Environment for Interactive Tasks in Large Realistic Scenes,” in *2021 IEEE/RSJ International Conference on Intelligent Robots and Systems (IROS)*, pp. 7520–7527.
- [18] E. Coumans and Y. Bai, “Pybullet: Physics simulation for games visual effects robotics and reinforcement learning.” [Online]. Available: <http://pybullet.org>